Adsorption of Cr(VI) ion on tannic acid/graphene oxide composite aerogel: kinetics, equilibrium, and thermodynamics studies

Chen Cheng[1] · Mengying Jia[1] · Linlin Cui[1] · Yue Li[1] · Lanshu Xu[1] · Xiaojuan Jin[1]

Abstract
A novel tannic acid–reduced graphene oxide (TAG) composite absorbent was prepared by using a simple one-step method. The prepared TAG was characterized by various analytical techniques including FTIR, Brunauer–Emmett–Teller (BET), scanning electron microscopy, X-ray diffraction, and X-ray photoelectron spectroscopy. Tannic acid (TA) not only can prevent graphene sheets from agglomerating by suppressing the hydrophobic stacking interactions but also can introduce a large number of phenol hydroxyls. The adsorption studies indicate that the TAG composite showed an excellent uptake capacity (179.22 mg/g) for Cr(VI) under the optimized conditions (viz., adsorbent dosages of 0.75 g/L, solution pH of 2.5, contact time of 360 min, and temperature of 60 °C), which is higher than that of most graphene oxide– and TA-based adsorbents. The BET specific surface area of TAG was calculated to be 118.3 m^2/g; the pore diameter of Tannin acid-reduced graphene hydrogel (TAGH) was mainly 3–6 nm, with pore size peak at 5.0 nm. The kinetics of Cr(VI) adsorption on TAG followed the pseudo-second-order model. The isotherm studies confirmed that the Cr(VI) chemically adsorbed on TAG in a monolayer fashion, which was attributed to the electrostatic interaction between chromium ions and oxygen negative ions. The process of Cr(VI) adsorption was found to be thermodynamically spontaneous and endothermic.

Keywords Tannic acid–decorated graphene · Adsorption of Cr(VI) · Kinetics model · Adsorption isotherms

1 Introduction

Since the industrial revolution, humankind has changed the world at an unprecedented speed and scale. While creating enormous wealth, the industry has also devastated the environment on which human beings depend. As an important environmental element for human survival and development, the water body has suffered from various types of pollution to varying degrees [1]. Heavy metal is a major environmental pollutant, which is highly toxic, degrading difficultly, and accumulating easily. It not only will damage the aquatic environment but also have the potential danger of harming aquatic organisms and human health through the food chain, which is of great concern worldwide [2]. Particularly, chromium, identified as one of the toxic pollutants that cause serious

environmental and public health problems, is often used in excess in industrial processes, such as tanning and electroplating, leather tanning, and corrosion protection painting; chromium pollution of source water represents an important environmental issue [3, 4].

Chromium exists mainly in two stable valence states of Cr(III) and Cr(VI) in the environment. Among them, Cr(III) is an essential element required by the human body, and its toxicity is relatively low, while Cr(VI) is chemically active, is easy to move, and has strong and long-lasting biological toxicity. In addition, it is easily absorbed by plants and poisons them [5]. Therefore, when the chromium-containing wastewater with excessive content is mixed into agricultural irrigation or water culture, it will enter the human body through the food chain, which is irritating to human skin and mucous membranes, and may cause cancer and seriously threaten human health [6–8]. The current treatment methods for removing hexavalent chromium include chemical precipitation, ion exchange, electrochemical, and adsorption [9]. Compared with other methods, the adsorption method has the advantages of high efficiency, energy saving, recycling, and environmental protection.

✉ Xiaojuan Jin
jxj0322@163.com

1 MOE Engineering Research Center of Forestry Biomass Materials and Bioenergy, Beijing Key Laboratory of Lignocellulosic Chemistry, Beijing Forestry University, Beijing 100083, China

Activated carbon and biochar are usually used as one of the common adsorbents for heavy metal pollution in water due to their large specific surface area. However, these carbon materials themselves usually contain less active groups, and it is difficult to efficiently remove hexavalent chromium in water. Therefore, researchers often modify it to obtain larger adsorption capacity and rate. Sun et al. [10] used cellulose and Fe (NO$_3$)$_3$ as the precursors of carbon and iron, respectively, and heated the precursor to 800 °C at a temperature increase rate of 10 °C/min to prepare magnetic carbon materials for removing Cr(VI). The material has a large specific surface area (136.27 m^2/g) and can separate the adsorbent from the solution by applying an external magnetic field. Lashanizadegan et al. [11] chemically activated chestnut shells by H$_3$PO$_4$ and carbonized them at 450 °C to prepare micro-mesoporous activated carbon adsorbents. The maximum adsorption capacity of Cr(VI) was 85.47 mg/g at a pH of 2.0.

Graphene (G) is a new type of carbonaceous material; its unique structure makes it exhibit many excellent properties. The theoretical value of up to 2630-m^2/g specific surface area, as well as a large number of unbonded π-electrons capable of bonding with electrons in heavy metals and aromatic organics [12], makes graphene a highly promising adsorbent for heavy metal and organic pollutant. However, due to the strong hydrophobic stacking and van der Waals force between the two-dimensional graphene sheets, graphene is easily agglomerated in an aqueous solution, thereby reducing the specific surface area of graphene and hindering the application of graphene in water pollutants. Graphene oxide (GO) is a product of chemical oxidation and stripping of graphite powder; it can be uniformly dispersed in an aqueous solution or other organic solvent. Some studies have shown that the performance of GO in the removal of pollutants from water can be improved by functionalization of GO with a number of reagents [13–19].

Recently, giving the graphene material a higher specific surface area and pore structure, the three-dimensional (3D) structured GO was a significant advancement in catalysts and environment applications [20–22]. This graphene material not only retains the high surface area of graphene sheets but also has a high pore structure network with a pore size of several micrometers. This unique structure gives it great potential in water treatment and has achieved great success, [23–28] but still requires a higher adsorption capacity and low-cost three-dimensional graphene composite.

Tannin is a widely distributed secondary metabolite of higher plants with a large amount of phenolic hydroxyl groups in its structure [29]. The rich catechol and pyrogallol units in the tannin molecule impart their reducing power, which is often used as a reducing agent for metal ions [30]. Tannic acid (TA) is one of the typical hydrolyzable tannins and can be used as a reducing agent and stabilizer for GO. Therefore, tannic acid can interact with multiple graphene nanosheets via hydrophobic interactions to form a network in solution, which possibly function as a template during the self-assembly of graphene nanosheets into a 3D architecture.

In this work, a high-performance and self-assembled graphene hydrogels were prepared with TA molecules as the reducer, stabilizer, and dispersant. Compared with other types of hexavalent chromium adsorbent [31–35], TA not only can prevent graphene sheets from agglomerating by suppressing the hydrophobic interactions in tannic acid–reduced graphene oxide (TAG) but also can introduce a large number of hydroxyls. The effects of pH, amount of adsorbent, initial concentration of heavy metal solution, and adsorption time on adsorption capacity were investigated. In addition, the kinetic and thermodynamic parameters of the adsorption process are determined, and different adsorption isotherm models are fitted to understand the adsorption behavior.

2 Experimental

2.1 Preparation of GO

GO sheets were prepared from graphite using the modified Hummers method [36]. Three grams of flake graphite and 1.5 g of sodium nitrate were stirred in an ice water bath of 70 mL of 98% H$_2$SO$_4$ for 15 min, and then a total of 9 g of potassium permanganate and 3 g of potassium ferrate were slowly added in three batches, with an interval of 15 min between each batch. After the addition of the drug, the solution was stirred for an additional 90 min in an ice water bath, then the beaker was transferred to a water bath and stirred for 3 h at 30–40 °C. A total of 150 mL of deionized water was slowly added to the solution. The beaker was transferred to an oil bath at 90 °C for 20 min, then the oil bath was remove, 500 mL of deionized water was added to stir evenly, and 15 mL of 30% hydrogen peroxide was quickly added, and the color of the solution changed from dark brown to bright yellow. Finally, it was washed once with 250 mL of hydrochloric acid having a solubility of 1:10, and then washed with deionized water until the pH of the solution reached neutral, that is, a graphene oxide solution was obtained.

2.2 Preparation of TAG

The adsorbent used in the experiment was prepared by using the hydrothermal method using graphene oxide and tannic acid. A total of 100 mg of tannic acid was dissolved in 20 mL of graphene oxide solution having a concentration of 2 mg/mL in a ratio of 5:2. The mixture was sonicated for 20 min to be dispersed, placed in a polytetrafluoroethylene-lined autoclave and sealed, and kept at 180 °C for 12 h. The obtained hydrogel was freeze-dried for 24 h to obtain a tannic acid/graphene oxide composite aerogel (TAG).
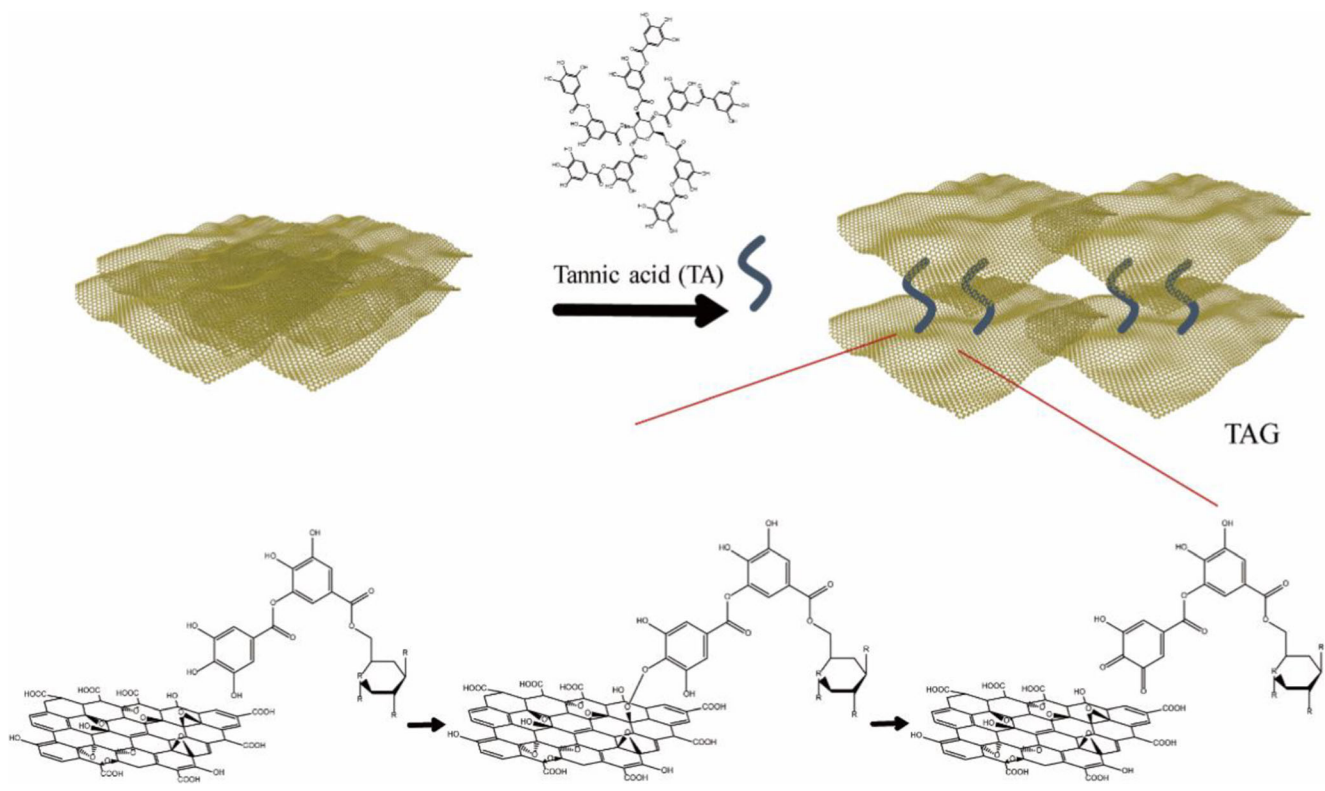
Fig. 1 Schematic illustration of reduction of GO by TA and macrostructure of TAG [37]

2.3 Adsorption experiments

All experiments were carried out at room temperature, 20 mL of the test solution was placed in a 100-mL centrifuge tube, and the adsorbent was placed. The bulk adsorption study was carried out under the desired pH, contact time, and adsorbent dosage. The Cr(VI) ion stock solution was prepared by dissolving 0.2829 g of potassium dichromate in 1000 mL of deionized water and adjusting the initial pH of the solution by adding an appropriate amount of 1 mol/L NaOH and HCL. The appropriate amount of adsorbent and initial concentration of the Cr(VI) solution were found by adding different doses of adsorbent and different initial concentrations of the Cr(VI) solution. Samples were taken at specified intervals until the equilibrium is reached to find the time to reach equilibrium. The filtrate from which the adsorbent was filtered was collected, and the residual chromium ion concentration in the filtrate sample was analyzed by following a standard method using a UNICO-UV-2600 ultraviolet-visible spectrophotometer and 1,5-diphenylcarbazide. The amount of adsorption of Cr(VI) per unit mass of adsorbent was calculated by using the following mass balance equation:

$$q = \frac{(c^0 - c^e)v}{w} \tag{1}$$

where C^0 is the initial concentration of Cr(VI), C^e is the concentration of h Cr(VI) in the solution at equilibrium, v is the volume of the Cr(VI) solution, and w is the dosage of the adsorbent.

3 Results and discussion

3.1 Characterization of TAG (Fig. 1)

Figure 2 shows the FTIR spectra of TA, G, and TAG. G exhibits several absorption bands at 3445, 1716, 1558, 1384,
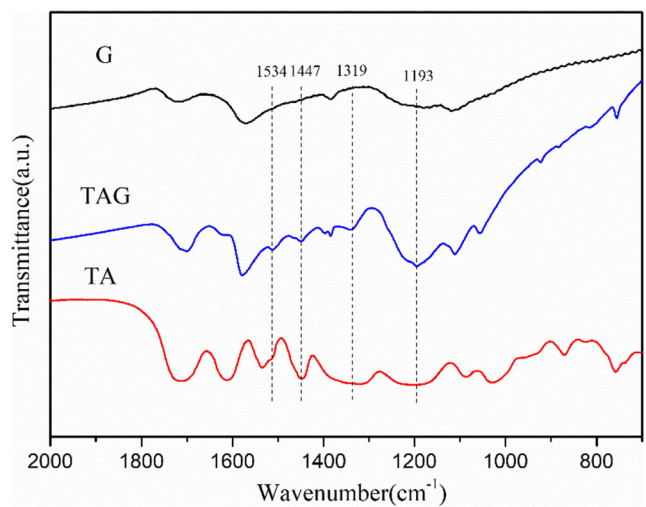

Fig. 2 FTIR spectra of TA, GO, and TAG

and 1110 cm^{-1}, which are attributed to the O–H stretching vibration, C=O stretching vibration, aromatic C=C stretching vibration, and C–O stretching vibration, respectively. For TAG, several new peaks at 1534, 1447, 1319, and 1193 cm-1 were observed, which were assigned to the characteristic bands of tannic acid, indicating that TA molecules have existed in graphene hydrogel. In previous literature [38], the reduction of GO can be directly reflected from the remarkable decrease in band intensity at 1730, 1380, and 1050 cm^{-1} with the removal of the most oxygen-containing group during chemical reduction. In our system, owing to the overlap of absorption bands of TA with those of GO, the reduction of GO could not get direct support from the FTIR spectrum, so it is necessary to combine the data of XPS to judge.

Determination of specific surface area and three-dimensional porous characteristics of the adsorbent TAG by nitrogen adsorption/desorption experiments. It can be clearly seen from Fig. 3 that TAG exhibits a type IV adsorption isotherm curve and an H4-type hysteresis loop. It indicates that the sample contains a large number of mesopores which structures are irregular [39]. The BET specific surface area of TAG was calculated to be 118.3 m^2/g, the pore diameter of TAGH was 3–6 nm, with pore size peak at 5.0 nm. TAG with low density had a lower specific surface area than that of GO, which might be attributed to the incorporation of the low surface area material of TA molecules. TA reduces the number of micropores in graphene itself in spite of expanding the graphene sheet structure [40]. As a result, the specific surface area of TAG has slightly reduced.

The SEM images of G and TAG are shown in Fig. 4. It can be observed that graphene sheet showed a typical wrinkled and crumbled two-dimensional structure. In contrast, from the surface images, TAG shows a 3D porous structure formed by the highly interconnected sheets with the presence of dominant large pores (the size ranging from 3 to 6 nm). Compared with G, we can see that larger mesopores were formed, and the pore walls became thinner in TAG, which could be explained

by the fact that the pore walls of the TA-decorated graphene hydrogel were highly etched, and some micropores collapsed as the TA molecules were a reducer itself. Combined with the results of BET, it is proved that the introduction of tannins does reduce the number of micropores, thereby reducing the surface area of TAG.

The XRD spectra of G showed two broad diffraction peaks at $2\theta = 24.2°$ ($d = 0.37$ nm) and 43.2° ($d = 0.21$ nm) corresponding to the reflection peak of (002) and (100) crystal planes of graphene (Fig. 5) [41]. As for TAG, a slightly sharp peak at around 26.3° with an interlayer space of 0.338 nm was quite close to that of natural graphite, indicating the successfully reduced TA and restored conjugate structures in TAG composites. Moreover, the intensity of the peak at $2\theta = 43.2°$ in TAG was weaker than that in G, which implied the intercalation of TA molecules among stacked graphene sheets [42].

The XPS was carried out to evaluate the surface elemental compositions of as-prepared samples (Fig. 6). The C 1s ($\sim$ 285.5 eV) and O 1s ($\sim$ 533 eV) both appear in the spectra of all as-prepared samples (Fig. 4a). The O content (20.56%) is dramatically reduced in TAG, due to the deoxygenation accompanied by translation of GO into graphene and the interactions between G and TA during hydrothermal assembly [43]. The C 1s peaks of G, TA, and TAG can be deconvoluted into four components, denoted as C=C/C–C (284.5 eV), C–O (286.6 eV), and C=O (289 eV). The content ratio of the C–O peak for TAG (29.4 at.%) is apparently less than that for TA (38.9 at.%) and GO (after the hydrothermal process), while the content ratio of the C=C/C–C peak increases. The results are attributed to the deoxygenation of GO during the hydrothermal process [44] and successful synthesis of TA/graphene composite, indicating that a hydrophobic conjugated structure is generated between the G and TA molecules after the introduction of TA [45]. The C=O content in TAG (10.2 at.%) is higher than that in G (5.4 at.%), suggesting the existence of quinoid functional groups by the introduction of TA [46, 47].
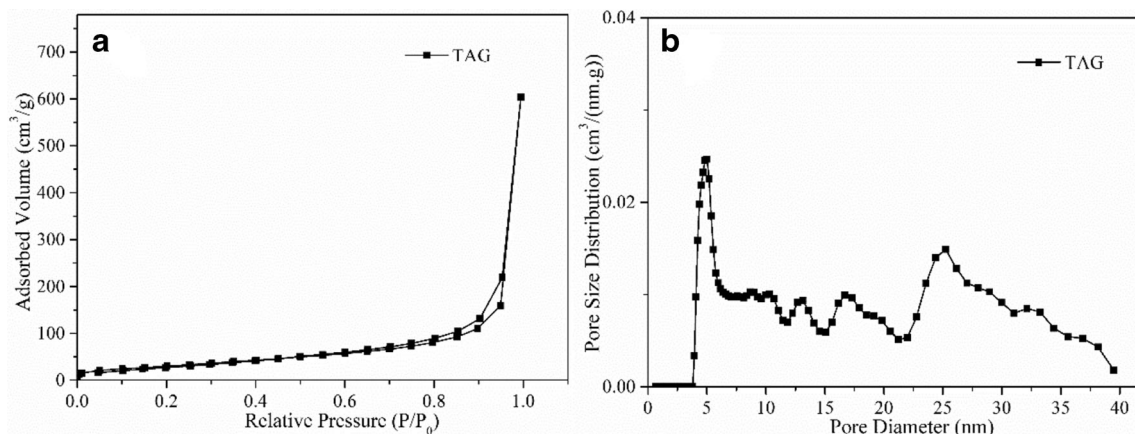
Fig. 3 **a** N$_2$ adsorption−desorption isotherms of TAG. **b** Pore size distribution of and TAG calculated by using the DFT method in nitrogen adsorption
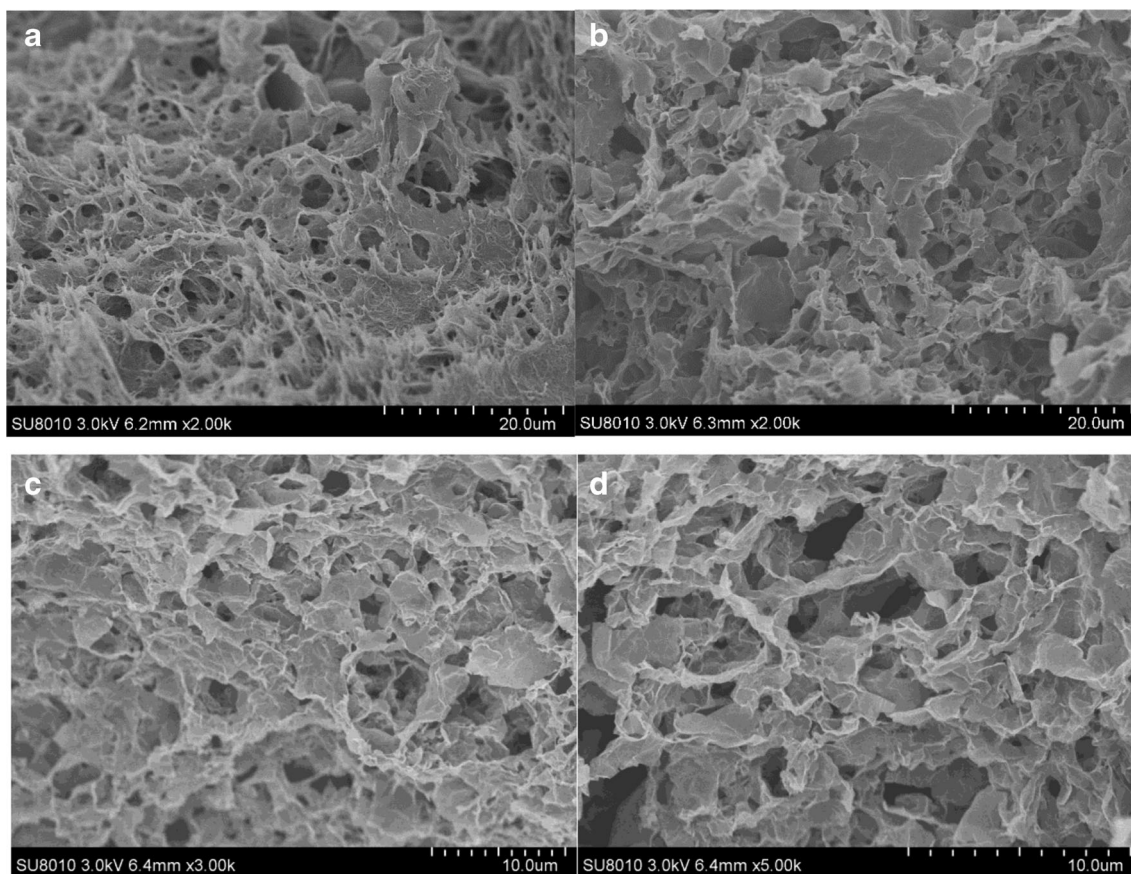
Fig. 4 SEM images of G (**a**, **c**) and TAG (**b**, **d**)

3.2 Effect of pH

It can be seen that as the pH increases, the amount of adsorption decreases, indicating that the pH of the solution has a great influence on the adsorption of Cr(VI) by TAG. The effect results are shown in Fig. 7.
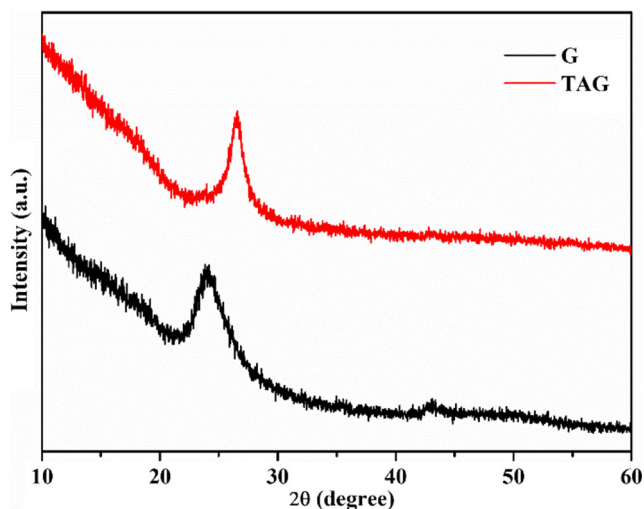

Fig. 5 XRD images of G and TAG

During the adsorption process, the pH of the solution affects not only the existence of hexavalent chromium but also the charge properties of the adsorbent surface. With the change of pH, hexavalent chromium ions coexist in aqueous solution mainly in the form of A, B, and C. H_2CrO_4 predominates at pH < 1.0, $HCrO^-_4$ at a pH range of 1.0–6.0, and CrO^{2-}_4 at pH > 6.0 [48]. By measuring the zeta potential of the adsorbent at different pHs, it is found that the point of zero charge (pH_{pzc}) of the adsorbent is at a pH of about 2.5.

The abundant acidic surface functional groups on TAG are protonated and positively charged in the forms of $-OH^+_2$, $-COOH^+_2$, or $=C=OH^+_2$ in the acidic medium. These protonated surface functional groups provide a more favorable electrostatic force of attraction for chromium anions ($HCrO^-_4$ or CrO^{2-}_4). Complexes form between adsorbents and adsorbates due to electrostatic attractive power, which causes chemical adsorption [49]. Thus, the more cations that exist on the surface of TAG, the better the adsorption capacity of Cr(VI) from water is. When the pH falls below pH_{pzc} (2.5), the surface of TAG possesses electropositivity, and it will transform to electronegativity gradually with increasing initial pH, leading to repulsion between the surface of TAG and chromium anions [48]. In an
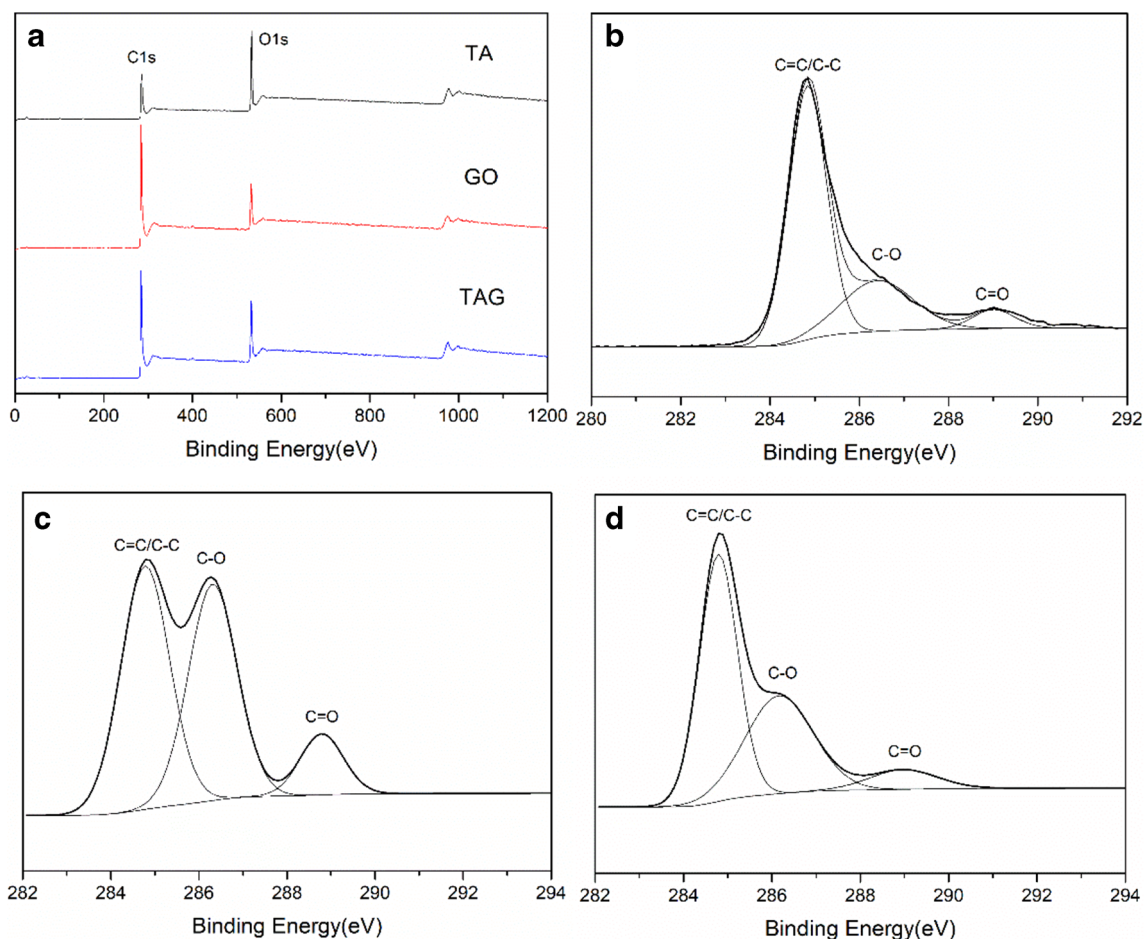
**Fig. 6** **a** XPS survey spectra of G, TA, and TAG. High-resolution XPS C 1s spectra of G (**b**), TA (**c**), and TAG (**d**)

alkaline environment, there will be a large amount of OH^- in the solution, and a large amount of OH^- can compete with the anion form of Cr(VI) for the adsorption sites on the TAG surface, thus greatly reducing the removal rate of Cr(VI). [50]

In addition, some Cr(VI) are reduced to Cr(III) during the adsorption process. The specific electron transfer process is as follows [51]:

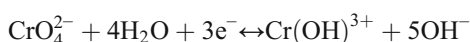$$HCrO_4^- + 7H^+ + 3e^- \leftrightarrow Cr^{3+} + 4H_2O$$
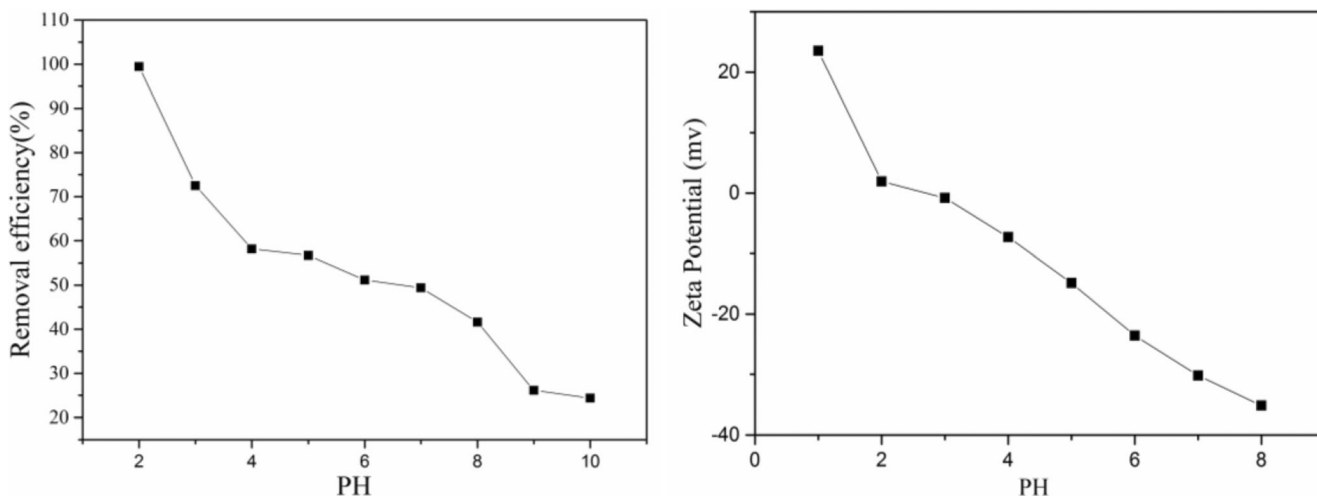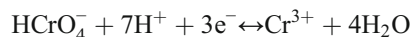
Fig. 7 Effect of pH on Cr(VI) adsorption (initial concentration of Cr(VI) is equal to 2 mg/L, TAG = 15 mg, volume = 20 mL, 298 K). Zeta potential at different pHs

Fig. 8 Three coordination complexes (**a**, **b**, **c**) formed by phenolic hydroxyl and chromium ions on TAG
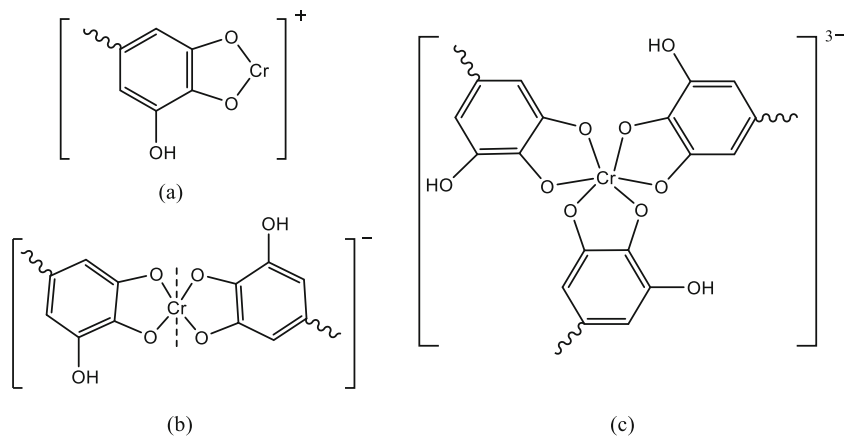
The reduction of CrO2–4 generates OH⁻:

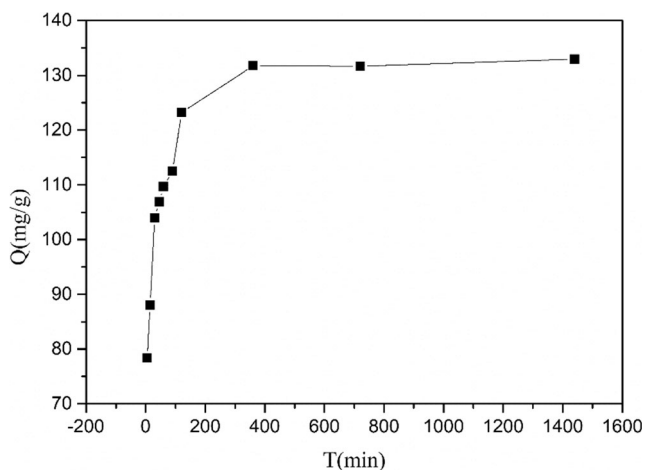$$CrO_4^{2-} + 4H_2O + 3e^- \leftrightarrow Cr(OH)^{3+} + 5OH^-$$

Carboxyl and phenolic hydroxyl are the dominant surface functional groups in TAG, and Cr(III) could be combined by ion exchange with these groups (Fig. 8).

3.3 Kinetics study

Figure 9 shows the adsorption of Cr(VI) ions to the adsorption time of the adsorbent.

It can be seen that the adsorption of Cr(VI) by the adsorbent gradually accumulates with time and reaches the adsorption equilibrium in the reaction for about 6 h. Nearly 90% of the hexavalent chromium was adsorbed in the first 2 h. This is because the amount of pore channels and functional groups on the surface of the adsorbent is sufficient at the initial stage of adsorption, and it is easier to combine heavy metal ions. As the reaction progresses, the active binding site decreases and

the concentration of heavy metal ions decreases, which gradually reaches the so-called adsorption equilibrium [52].
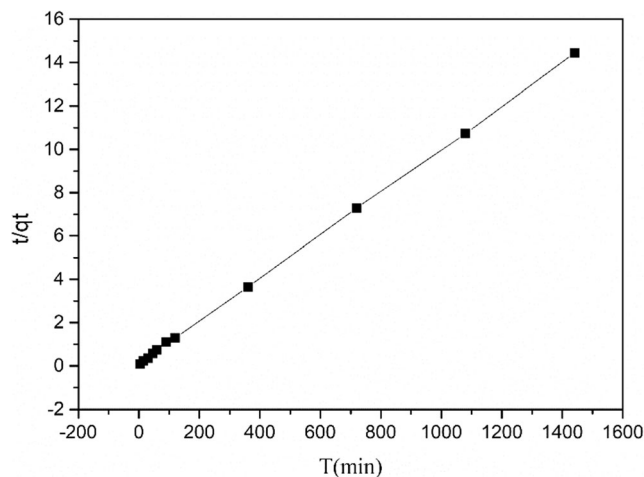
In order to further study the adsorption mechanism, the pseudo-1st-order equation (Eq. (2)) and the pseudo-2nd-order equation (Eq. (3)) were used to fit the adsorption data of the whole adsorption period.

$$ln(q_e - q_t) = lnq_e - k_1 t \tag{2}$$

$$\frac{t}{q_t} = \frac{1}{k_2 q_e} + \frac{t}{q_e} \tag{3}$$

where q_e (mg/g) is the equilibrium adsorption amount, q_t (mg/g) is the adsorption amount of TAG at time t (min), and k_1 and k_2 are the rate constant of the pseudo-1st-order model and the pseudo-2nd-order model (min⁻¹), respectively.

Figure 10 is a linear pseudo-2nd-order equation model curve of adsorbent adsorbing hexavalent chromium ions. Compared with quasi-first-order kinetics, the correlation coefficient of quasi-secondary kinetics is higher, and the q_e value calculated by quasi-secondary kinetics is consistent with the experimentally measured data. It is indicated that the adsorption process of sorbent to Cr(VI) satisfies the assumption of 2nd-order kinetics, and the rate-limiting step is a chemical

Fig. 9 Effect of time on TAG adsorption of Cr(VI) (initial concentration of Cr(VI) is equal to 2 mg/L, TAG = 15 mg, volume = 20 mL, 298 K, pH = 2.5)

Fig. 10 Pseudo-2nd-order plot for the adsorption of Cr(VI) by TAG

Table 1 Langmuir isotherm model parameters for TAG adsorption of hexavalent chromium

Pseudo-first-order kinetic model			Pseudo-second-order kinetic model		
$k_1(min^{-1})$	q_e (mg/g)	R^2	k_2 (g/mg*min)	q_e (mg/g)	R^2
0.24	125.68	0.83	$2.2*10^{-3}$	130.27	0.91

Table 2 Isotherm constants for TAG adsorption of hexavalent chromium

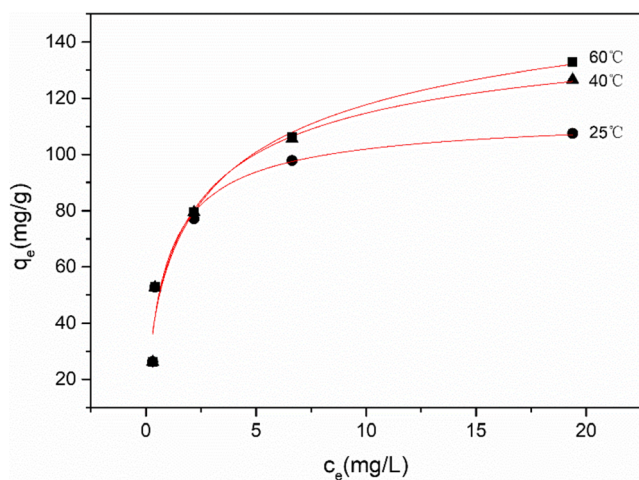| Absorbents	Langmuir model			Freundlich model		
$T(°C)$	q_m (mg/g)	K_L (L/mg)	R^2	K_F (L/mg)	n	R^2
25	115.32	0.51	0.90	85.42	4.25	0.89
40	154.94	0.73	0.93	107.79	6.76	0.90
60	179.22	0.65	0.93	120.35	4.69	0.88

process. This indicates that the speed-limiting step of adsorption may be due to chemical adsorption, which is mainly due to the high specific surface area of the adsorbent material and small internal diffusion resistance [53–56].

3.4 The adsorption isotherms

The adsorption isotherm for removing Cr(VI) was studied using a Cr(VI) solution with an initial concentration of 20 to 100 mg/L under the conditions of 0.75 mg/mL of adsorbent. The adsorption isotherm curve refers to the relationship between the concentration of solute molecules in the two phases when the adsorption process of the solute molecules at the two-phase interface reaches equilibrium, which provides information on the surface properties and adsorption behavior of the adsorbent, providing a reliable basis for further exploration of the adsorption mechanism. The experimental data obtained were fitted to the Langmuir adsorption isotherm (Table 1) [57]. The expression is as follows:

$$\frac{C_e}{q_e} = \frac{1}{K_L q_{max}} + \frac{C_e}{q_{max}^2} \qquad (4)$$

where C_e is the equilibrium concentration of the Cr(VI) solution, q_{max} is the maximum adsorption capacity of the adsorbent for the Cr(VI), q_e is the adsorption amount of the

Cr(VI) ion per unit mass of the dry adsorbent at the equilibrium of adsorption, and K_L is the Langmuir constant related to the affinity of the adsorption site.

Figure 11 shows the results of fitting the adsorption data to the Langmuir isotherm model. The relevant calculation parameters are shown in Table 2.

Compared with other adsorption models such as Freundlich, the correlation coefficient of the Langmuir model is higher, which is more suitable for the isotherm adsorption data of Cr(VI) by adsorbent materials. It is indicated that Cr(VI) is adsorbed on the surface of TAG by a single layer.

It is observed that the percentage removal of Cr(VI) was increased with an increase in the temperature from 40 to 60 °C, which may be due to the increase in diffusion rate of the metal ion [58]. The enhancement in removal efficiency with the increase in temperature may be attributed to the fact that at higher temperature, the energy of the system accelerates Cr(VI) attachment onto the adsorbent surface. In addition, as the temperature increases, q_m and K_L in the Langmuir model also increase, indicating that this reaction process is endothermic [59].

3.5 Thermodynamics for adsorption

The adsorption process of hexavalent chromium is a reversible process with heterogeneous equilibrium. Through thermodynamic studies, the feasibility of the adsorbent and the spontaneity of the adsorption process can be judged. Thermodynamic parameters can be calculated by using the following equation:

$$\Delta G^0 = -RT ln K^0 \qquad (5)$$

Fig. 11 Nonlinear Langmuir isotherm model for hexavalent chromium adsorption at 25 °C, 40 °C, and 60 °C by TAG

Table 3 Thermodynamic parameters for adsorption of Cr(VI) by TAG

T (K)	ΔG^0 (kJ/mol)	ΔH^0 (kJ/mol)	ΔS^0 (kJ/(K·mol))
298	− 17.67	4.87	70.35
313	− 20.38		
333	− 23.46		

Table 4 Comparison of adsorption capacities of the adsorbents for the removal of Cr(VI) with those of other adsorbents

Adsorbent	Specific surface area ($m^2 g^{-1}$)	Adsorption capacities (mg/g)	Reference
GO–nZVI	170	162	[61]
Cyclodextrin–chitosan–modified GO	445.6	61.31	[61]
GO–Mg(OH)$_2$	40	117.5	[62]
WHB–GO	25.89	150.02	[63]
TAG	118.3	179.22	This study

$$ln K^0 = -\frac{\Delta H^0}{RT} + \frac{\Delta S^0}{R} \qquad (6)$$

where ΔG^0 represents Gibbs free energy change, ΔH^0 represents metamorphosis, and ΔS^0 represents entropy change. The calculation results of thermodynamic parameters under three different temperature conditions are shown in Table 3.

It can be seen that the Gibbs free energy change ΔG^0 is negative, and as the temperature increases, the absolute value increases, indicating that the adsorption reaction process is a spontaneous reaction [60]. ΔH^0 (4.87) is a positive value, indicating that the adsorption process is an endothermic reaction, which is consistent with the previous research results of isothermal adsorption. ΔS^0 (70.35) is also a positive value, indicating that the adsorption process of Cr(VI) by TAG is spontaneously completed.

3.6 Comparison of Cr(VI) removal with different adsorbents reported in literature

As shown in Table 4, the adsorbent has better adsorption effect than other adsorbents.

4 Conclusions

In summary, a novel TAG composite aerogel with a 3D porous structure was successfully prepared via a simple one-step method. TA molecules not only can be fully competent in reducing graphene oxide and stabilizing reduced graphene oxide but also can be used as a dispersant and prevent graphene sheets from agglomerating by suppressing the hydrophobic interactions. In addition, tannic acid itself has a rich hydroxyl group, which provides more adsorption sites to absorb metal ions and enhance the adsorption capacity of Cr(VI). The adsorption capacity of TAG was found to be strongly dependent on pH, and the maximum removal capacity reaches up to 179.22 mg/g at pH 2.0 when the component ratio of GO and TA is 2:5. The adsorption process is spontaneous and endothermic, and it well fits the Langmuir and pseudo-second-order kinetic models, validating that the adsorption behavior is a monolayer chemical adsorption process.

These TAG adsorbents with sufficient functionalities effectively addressed the problems of low adsorption capacity in water purification, exhibiting a bright future for their applications in heavy metal removal from the wastewater.

References

1. Shen H, Chen J, Dai H, Wang L, Hu M, Xia Q (2013) New insights into the sorption and detoxification of chromium(VI) by tetraethylenepentamine functionalized nanosized magnetic polymer adsorbents: mechanism and pH effect. Ind Eng Chem Res 52(36):12723–12732. https://doi.org/10.1021/ie4010805

2. Zhao Y, Zhao D, Chen C, Wang X (2013) Enhanced photoreduction and removal of Cr(VI) on reduced graphene oxide decorated with TiO2 nanoparticles. J Colloid Interface Sci 405:211–217. https://doi.org/10.1016/j.jcis.2013.05.004

3. Basha S, Murthy ZVP (2007) Kinetic and equilibrium models for biosorption of Cr(VI) on chemically modified seaweed, Cystoseira indica. Process Biochem 42(11):1521–1529. https://doi.org/10.1016/j.procbio.2007.08.004

4. Zou Y, Wang X, Khan A, Wang P, Liu Y, Alsaedi A, Hayat T, Wang X (2016) Environmental remediation and application of nanoscale zero-valent iron and its composites for the removal of heavy metal ions: a review. Environ Sci Technol 50(14):7290–7304. https://doi.org/10.1021/acs.est.6b01897

5. Zolgharnein J, Shahmoradi A (2010) Adsorption of Cr(VI) onto Elaeagnus tree leaves: statistical optimization, equilibrium modeling, and kinetic studies. J Chem Eng Data 55(9):3428–3437. https://doi.org/10.1021/je100157y

6. Bai X, Du Y, Hu X, He Y, He C, Liu E, Fan J (2018) Synergy removal of Cr (VI) and organic pollutants over RP-MoS2/rGO photocatalyst. Appl Catal B Environ 239:204–213. https://doi.org/10.1016/j.apcatb.2018.08.016

7. Ghosh S, Remita H, Basu RN (2018) Visible-light-induced reduction of Cr(VI) by PDPB-ZnO nanohybrids and its photoelectrochemical response. Appl Catal B Environ 239:362–372. https://doi.org/10.1016/j.apcatb.2018.08.034

8. Du X-D, Yi X-H, Wang P, Zheng W, Deng J, Wang C-C (2019) Robust photocatalytic reduction of Cr(VI) on UiO-66-NH2(Zr/Hf) metal-organic framework membrane under sunlight irradiation. Chem Eng J 356:393–399. https://doi.org/10.1016/j.cej.2018.09.084

9. Luo X, Wang C, Wang L, Deng F, Luo S, Tu X, Au C (2013) Nanocomposites of graphene oxide-hydrated zirconium oxide for simultaneous removal of As(III) and As(V) from water. Chem Eng J 220:98–106. https://doi.org/10.1016/j.cej.2013.01.017

10. Qiu B, Wang Y, Sun D, Wang Q, Zhang X, Weeks BL, O'Connor R, Huang X, Wei S, Guo Z (2015) Cr(VI) removal by magnetic

carbon nanocomposites derived from cellulose at different carbonization temperatures. J Mater Chem A 3(18):9817–9825. https://doi.org/10.1039/c5ta01227a

11. Niazi L, Lashanizadegan A, Sharififard H (2018) Chestnut oak shells activated carbon: preparation, characterization and application for Cr (VI) removal from dilute aqueous solutions. J Clean Prod 185:554–561. https://doi.org/10.1016/j.jclepro.2018.03.026

12. Nair RR, Blake P, Grigorenko AN, Novoselov KS, Booth TJ, Stauber T, Peres NM, Geim AK (2008) Fine structure constant defines visual transparency of graphene. Science 320(5881):1308. https://doi.org/10.1126/science.1156965

13. Chauke VP, Maity A, Chetty A (2015) High-performance towards removal of toxic hexavalent chromium from aqueous solution using graphene oxide-alpha cyclodextrin-polypyrrole nanocomposites. J Mol Liq 211:71–77. https://doi.org/10.1016/j.molliq.2015.06.044

14. Zhang B, Hu R, Sun D, Wu T, Li Y (2018) Fabrication of chitosan/magnetite-graphene oxide composites as a novel bioadsorbent for adsorption and detoxification of Cr(VI) from aqueous solution. Sci Rep 8(1):15397. https://doi.org/10.1038/s41598-018-33925-7

15. Chen D, Zhang H, Yang K, Wang H (2016) Functionalization of 4-aminothiophenol and 3-aminopropyltriethoxysilane with graphene oxide for potential dye and copper removal. J Hazard Mater 310:179–187. https://doi.org/10.1016/j.jhazmat.2016.02.040

16. Madadrang CJ, Kim HY, Gao G, Wang N, Zhu J, Feng H, Gorring M, Kasner ML, Hou S (2012) Adsorption behavior of EDTA-graphene oxide for Pb (II) removal. ACS Appl Mater Interfaces 4(3):1186–1193. https://doi.org/10.1021/am201645g

17. Qi Y, Yang M, Xu W, He S, Men Y (2017) Natural polysaccharides-modified graphene oxide for adsorption of organic dyes from aqueous solutions. J Colloid Interface Sci 486:84–96. https://doi.org/10.1016/j.jcis.2016.09.058

18. Wu Z, Zhong H, Yuan X, Wang H, Wang L, Chen X, Zeng G, Wu Y (2014) Adsorptive removal of methylene blue by rhamnolipid-functionalized graphene oxide from wastewater. Water Res 67:330–344. https://doi.org/10.1016/j.watres.2014.09.026

19. Wang Z, Lin F, Huang L, Chang Z, Yang B, Liu S, Zheng M, Lu Y, Chen J (2019) Cyclodextrin functionalized 3D-graphene for the removal of Cr(VI) with the easy and rapid separation strategy. Environ Pollut 254. https://doi.org/10.1016/j.envpol.2019.07.022

20. Bi H, Xie X, Yin K, Zhou Y, Wan S, He L, Xu F, Banhart F, Sun L, Ruoff RS (2012) Spongy graphene as a highly efficient and recyclable sorbent for oils and organic solvents. Adv Funct Mater 22(21):4421–4425. https://doi.org/10.1002/adfm.201200888

21. Song X, Chen Y, Rong M, Xie Z, Zhao T, Wang Y, Chen X, Wolfbeis OS (2016) A phytic acid induced super-amphiphilic multifunctional 3D graphene-based foam. Angew Chem 55(12):3936–3941. https://doi.org/10.1002/anie.201511064

22. Lu K-Q, Yuan L, Xin X, Xu Y-J (2018) Hybridization of graphene oxide with commercial graphene for constructing 3D metal-free aerogel with enhanced photocatalysis. Appl Catal B Environ 226:16–22. https://doi.org/10.1016/j.apcatb.2017.12.032

23. Chen Y, Chen L, Bai H, Li L (2013) Graphene oxide–chitosan composite hydrogels as broad-spectrum adsorbents for water purification. J Mater Chem A 1(6):1992–2001. https://doi.org/10.1039/c2ta00406b

24. Cong HP, Qiu JH, Yu SH (2015) Thermoresponsive poly(N-isopropylacrylamide)/graphene/Au nanocomposite hydrogel for water treatment by a laser-assisted approach. Small 11(9–10):1165–1170. https://doi.org/10.1002/smll.201401651

25. Gan L, Shang S, Hu E, Yuen CWM, S-x J (2015) Konjac glucomannan/graphene oxide hydrogel with enhanced dyes adsorption capability for methyl blue and methyl orange. Appl Surf Sci 357:866–872. https://doi.org/10.1016/j.apsusc.2015.09.106

26. Gao H, Sun Y, Zhou J, Xu R, Duan H (2013) Mussel-inspired synthesis of polydopamine-functionalized graphene hydrogel as

reusable adsorbents for water purification. ACS Appl Mater Interfaces 5(2):425–432. https://doi.org/10.1021/am302500v

27. Tiwari JN, Mahesh K, Le NH, Kemp KC, Timilsina R, Tiwari RN, Kim KS (2013) Reduced graphene oxide-based hydrogels for the efficient capture of dye pollutants from aqueous solutions. Carbon 56:173–182. https://doi.org/10.1016/j.carbon.2013.01.001

28. Varaprasad K, Jayaramudu T, Sadiku ER (2017) Removal of dye by carboxymethyl cellulose, acrylamide and graphene oxide via a free radical polymerization process. Carbohydr Polym 164:186–194. https://doi.org/10.1016/j.carbpol.2017.01.094

29. Hagerman AE, Riedl KM, Jones GA, Sovik KN, Ritchard NT, Hartzfeld PW, Riechel TL (1998) High molecular weight plant polyphenolics (tannins) as biological antioxidants. J Agric Food Chem 46(5):1887–1892

30. Huang X, Wu H, Liao X, Shi B (2010) One-step, size-controlled synthesis of gold nanoparticles at room temperature using plant tannin. Green Chem 12(3):395–399. https://doi.org/10.1039/b918176h

31. Mohamed AK, Mahmoud ME (2020) Nanoscale Pisum sativum pods biochar encapsulated starch hydrogel: a novel nanosorbent for efficient chromium (VI) ions and naproxen drug removal. Bioresour Technol 308. https://doi.org/10.1016/j.biortech.2020.123263

32. Mahmoud ME, Osman MM, Abdel-Aal H, Nabil GM (2020) Microwave-assisted adsorption of Cr(VI), Cd(II) and Pb(II) in presence of magnetic graphene oxide-covalently functionalized-tryptophan nanocomposite. J Alloys Compd:823. https://doi.org/10.1016/j.jallcom.2020.153855

33. Mahmoud ME, Amira MF, Seleim SM, Mohamed AK (2020) Amino-decorated magnetic metal-organic framework as a potential novel platform for selective removal of chromium (VI), cadmium (II) and lead (II). J Hazard Mater 381. https://doi.org/10.1016/j.jhazmat.2019.120979

34. Mahmoud ME, Abdou AEH, Sobhy ME (2017) Engineered nano-zirconium oxide-crosslinked-nanolayer of carboxymethyl cellulose for speciation and adsorptive removal of Cr(III) and Cr(VI). Powder Technol 321:444–453. https://doi.org/10.1016/j.powtec.2017.08.041

35. Mahmoud ME, Yakout AA, Abdel-Aal H, Osman MM (2015) Speciation and selective biosorption of Cr(III) and Cr(VI) using nanosilica immobilized-fungi biosorbents. J Environ Eng 141(4):04014079. https://doi.org/10.1061/(asce)ee.1943-7870.0000899

36. Hummers WS Jr, Offeman RE (1958) Preparation of graphitic oxide. J Am Chem Soc 80(6):1339–1339

37. Luo J, Lai J, Zhang N, Liu Y, Liu R, Liu X (2016) Tannic acid induced self-assembly of three-dimensional graphene with good adsorption and antibacterial properties. ACS Sustain Chem Eng 4(3):1404–1413. https://doi.org/10.1021/acssuschemeng.5b01407

38. Lim M-Y, Shin H, Shin DM, Lee S-S, Lee J-C (2016) Poly(vinyl alcohol) nanocomposites containing reduced graphene oxide coated with tannic acid for humidity sensor. Polymer 84:89–98. https://doi.org/10.1016/j.polymer.2015.12.048

39. Ji CC, Xu MW, Bao SJ, Cai CJ, Lu ZJ, Chai H, Yang F, Wei H (2013) Self-assembly of three-dimensional interconnected graphene-based aerogels and its application in supercapacitors. J Colloid Interface Sci 407:416–424. https://doi.org/10.1016/j.jcis.2013.06.054

40. Ma Z, Zhao X, Gong C, Zhang J, Zhang J, Gu X, Tong L, Zhou J, Zhang Z (2015) Preparation of a graphene-based composite aerogel and the effects of carbon nanotubes on preserving the porous structure of the aerogel and improving its capacitor performance. J Mater Chem A 3(25):13445–13452

41. Luo J, Zhong W, Zou Y, Xiong C, Yang W (2016) Preparation of morphology-controllable polyaniline and polyaniline/graphene hydrogels for high performance binder-free supercapacitor

electrodes. J Power Sources 319:73–81. https://doi.org/10.1016/j.jpowsour.2016.04.004

42. Lei Y, Tang Z, Liao R, Guo B (2011) Hydrolysable tannin as environmentally friendly reducer and stabilizer for graphene oxide. Green Chem 13(7):1655. https://doi.org/10.1039/c1gc15081b

43. Xiong C, Zou Y, Peng Z, Zhong W (2019) Synthesis of morphology-tunable electroactive biomass/graphene composites using metal ions for supercapacitors. Nanoscale 11(15):7304–7316. https://doi.org/10.1039/c9nr00659a

44. Tang CY, Yu P, Tang LS, Wang QY, Bao RY, Liu ZY, Yang MB, Yang W (2018) Tannic acid functionalized graphene hydrogel for organic dye adsorption. Ecotoxicol Environ Saf 165:299–306. https://doi.org/10.1016/j.ecoenv.2018.09.009

45. Xu Y, Sheng K, Li C, Shi G (2010) Self-assembled graphene hydrogel via a one-step hydrothermal process. ACS Nano 4(7):4324–4330

46. Milczarek G, Inganäs O (2012) Renewable cathode materials from biopolymer/conjugated polymer interpenetrating networks. Science 335(6075):1468–1471

47. Kim SK, Kim YK, Lee H, Lee SB, Park HS (2014) Superior pseudocapacitive behavior of confined lignin nanocrystals for renewable energy-storage materials. ChemSusChem 7(4):1094–1101. https://doi.org/10.1002/cssc.201301061

48. Monser L, Adhoum N (2009) Tartrazine modified activated carbon for the removal of Pb(II), Cd(II) and Cr(III). J Hazard Mater 161(1):263–269. https://doi.org/10.1016/j.jhazmat.2008.03.120

49. Huang G, Shi JX, Langrish TAG (2009) Removal of Cr(VI) from aqueous solution using activated carbon modified with nitric acid. Chem Eng J 152(2–3):434–439. https://doi.org/10.1016/j.cej.2009.05.003

50. Li W, Gong X, Li X, Zhang D, Gong H (2012) Removal of Cr(VI) from low-temperature micro-polluted surface water by tannic acid immobilized powdered activated carbon. Bioresour Technol 113:106–113. https://doi.org/10.1016/j.biortech.2011.12.037

51. Chand R, Narimura K, Kawakita H, Ohto K, Watari T, Inoue K (2009) Grape waste as a biosorbent for removing Cr(VI) from aqueous solution. J Hazard Mater 163(1):245–250. https://doi.org/10.1016/j.jhazmat.2008.06.084

52. Bishnoi NR, Bajaj M, Sharma N, Gupta A (2004) Adsorption of Cr(VI) on activated rice husk carbon and activated alumina. Bioresour Technol 91(3):305–307. https://doi.org/10.1016/s0960-8524(03)00204-9

53. Plazinski W, Rudzinski W, Plazinska A (2009) Theoretical models of sorption kinetics including a surface reaction mechanism: a review. Adv Colloid Interf Sci 152(1–2):2–13. https://doi.org/10.1016/j.cis.2009.07.009

54. Fan L, Zhang Y, Luo C, Lu F, Qiu H, Sun M (2012) Synthesis and characterization of magnetic beta-cyclodextrin-chitosan nanoparticles as nano-adsorbents for removal of methyl blue. Int J Biol Macromol 50(2):444–450. https://doi.org/10.1016/j.ijbiomac.2011.12.016

55. Kumar KV (2007) Pseudo-second order models for the adsorption of safranin onto activated carbon: comparison of linear and non-linear regression methods. J Hazard Mater 142(1–2):564–567. https://doi.org/10.1016/j.jhazmat.2006.08.018

56. Hubbe MA, Rojas OJ, Lucia LA (2015) Green modification of surface characteristics of cellulosic materials at the molecular or nano scale: a review. Bioresources 10(3):6095–6206

57. Langmuir I (1918) The adsorption of gases on plane surfaces of glass, mica and platinum. J Am Chem Soc 40(9):1361–1403

58. Nouri L, Ghodbane I, Hamdaoui O, Chiha M (2007) Batch sorption dynamics and equilibrium for the removal of cadmium ions from aqueous phase using wheat bran. J Hazard Mater 149(1):115–125. https://doi.org/10.1016/j.jhazmat.2007.03.055

59. Hu X-j, Wang J-s, Y-g L, Li X, G-m Z, Bao Z-l, X-x Z, A-w C, Long F (2011) Adsorption of chromium (VI) by ethylenediamine-modified cross-linked magnetic chitosan resin: isotherms, kinetics and thermodynamics. J Hazard Mater 185(1):306–314. https://doi.org/10.1016/j.jhazmat.2010.09.034

60. Bhattacharya A, Naiya T, Mandal S, Das S (2007) Adsorption, kinetics and equilibrium studies on removal of Cr(VI) from aqueous solutions using different low-cost adsorbents. Chem Eng J. https://doi.org/10.1016/j.cej.2007.05.021

61. Li L, Fan L, Sun M, Qiu H, Li X, Duan H, Luo C (2013) Adsorbent for chromium removal based on graphene oxide functionalized with magnetic cyclodextrin-chitosan. Colloids Surf B Biointerfaces 107:76–83. https://doi.org/10.1016/j.colsurfb.2013.01.074

62. Liu M, Xu J, Cheng B, Ho W, Yu J (2015) Synthesis and adsorption performance of Mg(OH)2 hexagonal nanosheet–graphene oxide composites. Appl Surf Sci 332:121–129. https://doi.org/10.1016/j.apsusc.2015.01.121

63. M-r S, Y-g L, S-b L, G-m Z, Tan X-f, L-h J, X-x H, Ding Y, Guo Y-m, Wang S-f (2016) A novel graphene oxide coated biochar composite: synthesis, characterization and application for Cr (VI) removal. RSC Adv 6(88):85202–85212